

Rheological regimes in agitated granular media under shear

Olfa D'Angelo,^{1,2,3} Matthias Sperl,^{3,4} and W. Till Kranz^{3,4}

¹*Institut Supérieur de l'Aéronautique et de l'Espace (ISAE-SUPAERO), Université de Toulouse, Toulouse, France*

²*Institute for Multiscale Simulation, Erlangen-Nürnberg Universität, Cauerstraße 3, 91058 Erlangen, Germany*

³*Institute of Materials Physics in Space, German Aerospace Center (DLR), Linder Höhe, 51170 Cologne, Germany*

⁴*Institute for Theoretical Physics, University of Cologne, Zùlpicher Straße 77, 50937 Cologne, Germany*

Agitated granular media have a rich rheology: they exhibit Newtonian behavior at low shear rate and density, develop a yield stress at high density, and cross over to Bagnoldian shear thickening when sheared rapidly—making them challenging to encompass in one theoretical framework. We measure the rheology of air-fluidized glass particles, spanning five orders of magnitude in shear rate. By comparing fluidization-induced to Brownian agitation, we show that all rheological regimes can be delineated by two dimensionless numbers—the Peclet number, Pe , and the ratio of shear-to-fluidization power, Π —and propose a constitutive relation that captures all flow behaviors, qualitatively and quantitatively, in one unified framework.

Systems out of equilibrium, which evolve or remain in a steady state through energy exchange with their environment, are widespread, yet poorly understood from a fundamental point of view. Such systems can be found at many length-scales, from biological matter, to colloidal suspensions, emulsions, up to traffic flow or even star-forming regions. In granular media, constant agitation counteracts the particles' dissipative nature, transforming static granular solids into dynamic granular fluids with a non-zero granular temperature T , i.e., a finite mean kinetic energy per particle [1, 2]. From industrial reactors [3, 4] to geophysical flows [5–8], granular media under constant agitation are widespread, but continue to be challenging to understand and describe theoretically.

Measuring the rheology of agitated granular media has yielded seemingly contradictory results. Considering a wide range of geometries and agitation mechanisms (air-fluidized [7–10], suspended in a liquid flow [11–14], tapped or vibrated [15–18], acoustically fluidized [6, 19, 20], combined air flow and vibrations [4]), some studies report Newtonian rheology [21–23] while others find shear thinning [24–26], and yet others shear thickening (Bagnoldian) rheology [10, 18, 27]—or crossovers between these behaviors [9, 14–16, 19, 28–31]. Yet, a succinct and comprehensive constitutive equation for agitated granular fluids, describing the stress tensor, Σ , as a function of shear rate, $\dot{\gamma}$, remains elusive.

In this Letter, we demonstrate that the rheology of agitated granular media actually encompasses all three regimes: Newtonian, shear thinning, and Bagnoldian shear thickening. By comparing fluidization-induced agitation to Brownian agitation, we extend arguments pertaining to colloidal suspensions to physically explain each regime. We show that the regime transitions are controlled by two dimensionless numbers: the Peclet number, Pe , and the ratio of shear-to-fluidization power, Π . Finally, we show that the granular integration through transient (GIT) [32, 33]—developed from mode-coupling theory (MCT), a first-principles-based theory for glassy dynamics [34, 35]—captures in one theoretical framework the

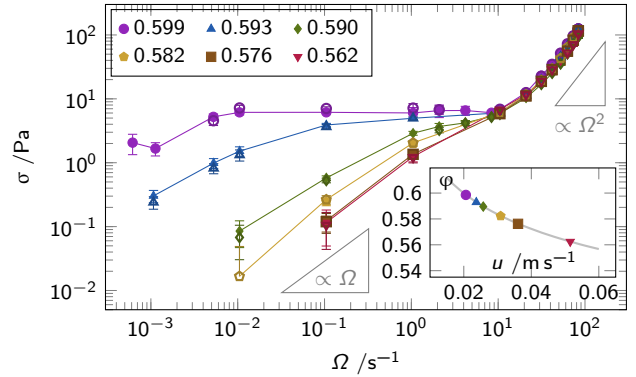


FIG. 1. Steady state flow curves, $\sigma(\Omega)$, for air-fluidized glass beads: shear stress, σ , vs. angular velocity, Ω , of the inner cylinder in a Taylor-Couette shear cell. Each flow curve corresponds to a packing fraction, φ , given in the legend. Filled marks correspond to the upward sweep, empty marks to the downward sweep in Ω . Lines are a guide to the eye. Inset: Global packing fraction vs. fluidization air flow velocity, $\varphi(u)$; the gray line is a fit to experimental data (details in Appendix I).

complex rheology of agitated granular media.

Experiments.—We measure the steady-state rheology of air-fluidized glass particles (glass bulk density $\rho_p = 2.5 \text{ g cm}^{-3}$, diameter $d \in [150\text{--}200] \mu\text{m}$, sample mass $M = 170 \text{ g}$, Geldart group B [1]), and vary the fluidization gas flow velocity, u . The single fluidization control parameter is u : the bed expands with increasing u , which lowers the global packing fraction, φ , (see Fig. 1 inset) and, at the same time, increases agitation. While $\varphi(u)$ characterizes the fluidized bed's density, its agitation can be characterized by the injected power density, $\Pi_f(u) = \rho_p \varphi u g$ (g gravitational acceleration). In the unsheared bed, Stokes numbers $St \gg 1$ [36], such that particles are not overdamped by the surrounding fluid (air), but driven by their inertia, forming a non-Brownian dry suspension.

The rheology of our air-fluidized granular bed is measured in a wide gap Taylor-Couette shear cell (Anton

Paar MCR-102, coaxial cylinders, geometry details in Appendix I). The torque, \mathcal{M} , for a fixed inner cylinder's angular velocity, Ω , is recorded and converted to stress, $\sigma = \mathcal{M}/2\pi LR_i^2$ (L and R_i inner cylinder height and radius, respectively). Steady state follows long transients (on the order of hours for slow shear). Flow curves, $\sigma(\Omega|\varphi)$, are plotted in Fig. 1, spanning five orders of magnitude in angular velocity for a range of packing densities.

Rheological regimes.—In Figure 1, we see that an air-fluidized granular bed may behave as a Newtonian fluid at low φ and Ω , as a shear thickening fluid at high Ω , or as a shear thinning fluid at intermediate Ω and at high φ . Similar regimes have been observed in molecular glasses and colloids [37–39]. We will argue below that while Bagnoldian shear thickening is genuinely granular, the Newtonian and shear thinning behaviors, including evidence of an incipient granular glass transition, may be understood in terms that generalize concepts developed for equilibrium fluids, highlighting a universality of fluid-like, amorphous materials across scales.

Newtonian rheology.—Characterized by the linear relation between shear stress and shear rate (or angular velocity), $\sigma \propto \Omega$, a Newtonian regime is observed at low shear and density. To translate the rotation rate, Ω , into the shear rate in the gap, $\dot{\gamma} = K_N \Omega$, we use the well-known strain constant $K_N = 2\delta^2/(\delta^2 - 1)$ (where $\delta = R_o/R_i$, ratio of outer to inner shear cell radii). As the velocity gradient depends on both shear geometry and fluid's rheology, different rheological regimes imply different strain constants; K_N encodes the Taylor-Couette geometry for Newtonian fluids (see Appendix II for full derivation). Plotting $\eta(\dot{\gamma}) = \sigma/\dot{\gamma}$ (Fig. 2a) exhibits this regime of constant viscosity, $\eta_N := \eta(\dot{\gamma} \rightarrow 0)$.

In this regime, fluidization dominates over shear. The dissipative collisions provide an energy sink with a power density $\Pi_c(T_0)$ that balances the fluidization, $\Pi_f = \Pi_c$, and fixes a constant granular temperature in the un-sheared state, T_0 . $\Pi_\dot{\gamma} := \sigma\dot{\gamma}$, remains negligible compared to the effect of fluidization, $\Pi_\dot{\gamma} \ll \Pi_f$, the granular temperature T_0 does not change appreciably [32]. Qualitatively, the rheology of the fluidized bed is the same as that of colloidal suspensions. From this analogy, Newtonian rheology is expected, with our shear rate independent viscosity, η_N , increasing with density [39–41].

As a function of packing fraction, we indeed measure a strong increase in Newtonian viscosity, $\eta_N(\varphi)$, captured by a power law divergence (Fig. 2b),

$$\eta_N(\varphi) \propto (\Phi - \varphi)^{-\gamma}. \quad (1)$$

For dense suspensions, Eq. (1) is known as the Krieger-Dougherty (K-D) relation [42], where $\Phi = \varphi_g$ denotes the maximal concentration of the suspension at which η_N diverges (here, $\varphi_g = 0.6$) and $\gamma = 2.5\varphi_g$ (dashed line in Fig. 2b). MCT can also be used to predict the divergence of η_N upon approaching a critical density, $\Phi = \varphi_c$, with $\varphi_c < \varphi_g$ [35, 41]. The system-specific parameter

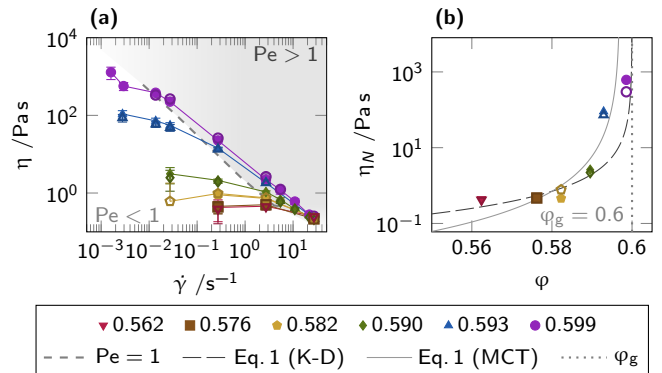


FIG. 2. Fluidized granular bed apparent viscosity, $\eta = \sigma/\dot{\gamma}$, in the Newtonian and shear thinning regimes. (a) Viscosity, $\eta(\dot{\gamma})$ vs. shear rate, $\dot{\gamma} = K_N \Omega$ (see text for details). Péclet number $Pe = 1$ (cf. Eq. 2) is indicated by the dashed line, $Pe > 1$ by shaded background. (b) Newtonian viscosity, η_N , averaged over the relevant $\dot{\gamma}$ for each packing fraction, φ ; the vertical dotted line indicates φ_g . Dashed line indicates Eq. (1) for the K-D relation; solid line Eq. (1) according to MCT predictions.

γ assumes $\gamma \approx 2.4$ [41], and $\varphi_c = 0.597$ (solid line in Fig. 2b). Above φ_c , the fluidized bed arrests into an amorphous solid, with all particles still agitated ($T_0 > 0$), but unable to move over long distances, due to the cage-like structure formed by their neighbors [2, 41, 43].

Dynamic yield stress.— While a true yield stress in suspensions has been subject to debate [38, 44], an apparent yield stress at low $\dot{\gamma}$ and high φ was since measured in emulsions [45], foams [46], colloidal [47] and granular suspensions [48]. At our highest packing fraction, $\varphi = 0.599 \lesssim \varphi_g$, we observe a well-defined plateau in the flow curves, from which we can extrapolate a finite dynamic yield stress, $\sigma_0 := \sigma(\varphi_g) \approx 6$ Pa, for the emerging granular glass.

In non-agitated granular solids, cohesive and frictional forces in lasting particle contacts result in a *static* yield stress [49–51]. By fluidization, contacts between particles are explicitly broken, such that particle interactions cannot explain the dynamic yield stress observed. Such dynamic yield stress at the transition to an amorphous solid is expected at the glass transition [32, 34, 52]. Due to the continuous agitation, particles stay in motion ($T_0 > 0$), even in the granular glass state. This is incompatible with a static ($T_0 = 0$), jammed configuration, with lasting particle-particle contacts. It is however perfectly compatible with a glassy state of matter, where local motion of a particle is permitted, but long range motion is suppressed by the cage-like structure formed by the particles' neighbors [2, 41, 43].

A $\varphi_g = 0.6$ is consistent with expectations. For colloidal suspensions in thermal equilibrium, $\varphi_g \simeq 0.57$ - 0.58 [53]. A higher φ_g for our agitated granular system can be

attributed to its characteristics: (i) polydispersity (within $1/4d$) allows denser packing [54], and (ii) dissipative particle collision require a higher critical density to solidify [41]. Hence, we identify φ_g as the density at a granular glass transition, distinct from a jamming transition.

Shear thinning rheology.—At intermediate $\dot{\gamma}$, a shear thinning regime appears, where η decreases with increasing $\dot{\gamma}$ (Fig. 2a).

In Brownian suspensions, shear thinning emerges when shear-induced particle motion becomes relevant compared to thermally activated diffusion. A finite diffusivity is related to a finite structural relaxation time, τ , that diverges with the viscosity, $\tau \sim \eta_N$. In our non-Brownian but constantly agitated air-fluidized bed, it is the imposed granular temperature that induces a time-scale, τ , competing with that of shear, $1/\dot{\gamma}$. The Péclet number captures this competition: $Pe \ll 1$ is associated with slow, fluidization-induced flow and $Pe \gg 1$ with shear dominated flow. In the latter case, the fluid structure can no longer instantaneously adapt to the imposed shear and effectively behaves as a yield stress fluid, resulting in a shear thinning rheology.

We define a proxy for the characteristic fluidization-induced time-scale, $\tau(\varphi) = \eta_N(\varphi)/\sigma(\dot{\gamma}_0|\varphi)$, by generalizing the yield stress to a typical stress value, $\sigma_0(\varphi) := \sigma(\dot{\gamma}_0|\varphi)$ [49–51, 55]. For the lower packing fractions, $\varphi \ll \varphi_g$, we use the stress at the flow curves' inflection point, $\sigma(\dot{\gamma}_0)$, at the end of the Newtonian regime. [56]. This allows us to calculate the corresponding Péclet number [57],

$$Pe := \eta_N(\varphi)\dot{\gamma}/\sigma(\dot{\gamma}_0|\varphi). \quad (2)$$

In Figs. 2a and 4 we find, indeed, $Pe \sim 1$ to trace the crossover from Newtonian to shear thinning behavior, generic for dense suspensions [34, 37, 38]. As long as shear-induced agitation is negligible, we find the analogy to colloidal suspensions to still hold.

Bagnoldian rheology.—The shear thickening regime appears once $\Omega \gtrsim 10 \text{ s}^{-1}$, and exhibits $\sigma \sim \Omega^2$ (see Fig. 1), a scaling first identified by Bagnold in granular suspension [27]. As the material's flow profile varies with its rheology, $\dot{\gamma}$ is related to the angular velocity, Ω , by a different strain constant, $K_B = \delta/(\delta - 1)$ (full derivation in Appendix II), that captures the specifics of our shear geometry, only now for a Bagnoldian instead of a classical Newtonian fluid. The data in Fig. 3 is plotted for $\dot{\gamma} = K_B\Omega$.

First, we want to assess whether Taylor vortices, previously observed in granular fluidized beds [58], and which could explain a significant increase in σ [59], might appear in our system. We calculate the gap Reynolds and Taylor numbers for the granular fluidized bed. The former, $Re = \rho_b \varphi R_i \Omega (R_o - R_i)/\eta$, compares the time-scale of rotational advection to that of viscous damping. It remains small throughout the experiment ($Re < 10$) (details in Appendix III), suggesting laminar flow [55, 60–63]. The Taylor number, Ta [64], compares Coriolis to viscous

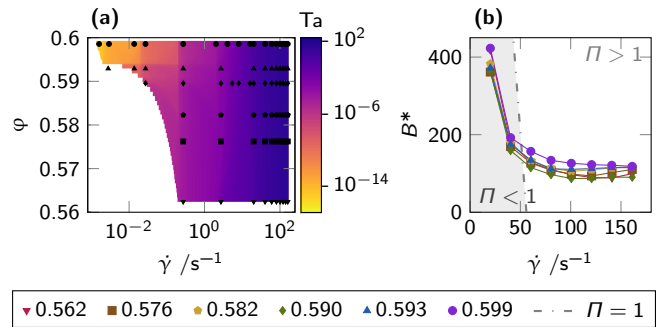


FIG. 3. Flow curves analysis for the high shear rate regime (where $\dot{\gamma} = K_B\Omega$, see text for details). (a) Taylor number, Ta , calculated on the full range of experimental data available. Location of measurements indicated by black dots. (b) Dimensionless Bagnold coefficients, B^* as a function of shear rate $\dot{\gamma}$ for the packing fraction as given in the legend. The dash-dotted line displays the location of power ratio $\Pi = 1$, marking the onset of the Bagnold regime

forces [61, 65]. Taylor vortices are expected to emerge if Ta exceeds a critical value, estimated around $Ta_c \sim \mathcal{O}(10^3)$ or above [61, 65, 66] (details in Appendix III). Fig. 3a shows that we do not achieve Taylor numbers higher than $Ta \lesssim 10^2 \ll Ta_c$, such that shear thickening cannot be explained by the Taylor instability.

Dense suspensions generally feature a shear thickening regime at high shear rates [38, 67, 68]. In Brownian suspensions, two primary mechanisms are associated with shear thickening: hydrodynamic effects and the lubrication-to-friction transition [67, 69–71]. But the shear thickening observed in the Bagnold regime has a different origin. While in Brownian suspensions, the interstitial fluid is in thermal equilibrium with the particles and can absorb the effect of shear heating, in the fluidized bed, the granular temperature is decoupled from the air's thermodynamic temperature. The granular temperature is hence immediately increased by shear heating, resulting in an increased shear stress.

The crossover to the Bagnold regime is expected once shear heating, $\Pi_{\dot{\gamma}}$, becomes comparable to the fluidization power density, Π_f , i.e., at a ratio

$$\Pi := \Pi_{\dot{\gamma}}/\Pi_f = \sigma\dot{\gamma}/\rho_b\varphi u g \quad (3)$$

of the order of one. In Figs. 3b and 4, we find that the power density ratio, Π , indeed controls the emergence of the Bagnold behavior.

Remark also that shear stress collapses for all φ once reaching the shear thickening regime (Figs. 1, 2a, 3b, 5a). We attribute this to shear dominating in this regime: fluidization-induced variations in packing density become negligible. The high $\dot{\gamma}$ regime is hence indeed Bagnold shear thickening, where $\dot{\gamma}$ becomes the only relevant time-scale in the system.

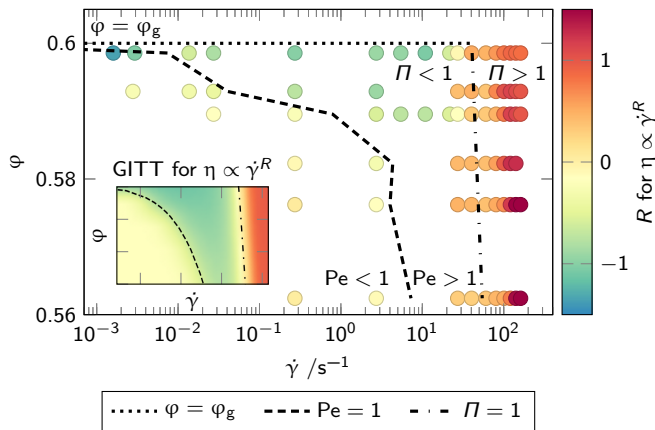


FIG. 4. Rheological state diagram spanned by packing fraction φ and shear rate $\dot{\gamma}$. The flow index R ($\eta \propto \dot{\gamma}^R$) is color coded, where $R = 0$ corresponds to Newtonian rheology and $R < 0$ ($R > 0$) indicates shear thinning (thickening) behavior. The dashed line traces Péclet number $Pe = 1$, and the dash-dotted line delineates power ratio $\Pi = 1$. The dotted line marks the granular glass transition at $\varphi_g = 0.6$.

The Bagnold regime and its emergence, specific to granular materials [72], have been studied in a number of contexts [73–75]; yet, quantitative measurements of Bagnold coefficients are limited. In Fig. 3b, we presents the Bagnold coefficients, $B = \sigma/\dot{\gamma}^2$, expressed in dimensionless form, as $B^* = Bd/m$ (d and m average particle diameter and mass). We find $B^* \sim \mathcal{O}(100)$ (averaged over the four highest shear rates) with no clear density dependence. We compare our results to Bagnold’s seminal measurements [27], where $0.1 < B^* < 10$, increasing with φ . The suspension used in [27] (wax spheres in liquids) shows higher dissipation, consistent with the smaller B^* , compared to glass beads in air.

At this point, let us summarize that the flow curves of our air-fluidized bed can be qualitatively characterized by two dimensionless numbers: the power ratio, Π , and the Péclet number, Pe (*cf.* Fig. 4). For $\Pi > 1$, the granular medium becomes purely shear driven—fluidization is negligible—and Bagnold rheology applies. For $\Pi < 1$, fluidization controls the granular temperature T_0 —shear is negligible—and, in complete analogy to Brownian suspensions, the rheology evolves with the Péclet number from Newtonian ($Pe \ll 1$) to shear thinning ($Pe \gg 1$).

Constitutive relation.—The granular extension of the integration through transients (ITT) formalism, GITT [32, 33], takes this scaling analysis into account to extract the divergent relaxation time, τ , as well as the power balance, to provide a dimensionless constitutive relation for dissipative smooth hard sphere.

Details about GITT are given in Appendix IV and elsewhere [32, 33]. The physical intuition behind this model is that of all stress relaxation modes, the slowest one in dense fluids will be the density fluctuations [34]. In the GITT

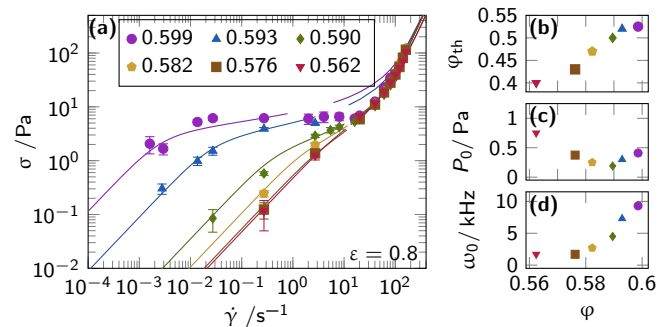


FIG. 5. (a) Constitutive relation (Eq. A8, solid lines) fitted to the experimental data (marks) in the Newtonian and Bagnold regime. The fit parameters (for coefficient of restitution $\varepsilon = 0.8$) are the theoretical packing fraction, φ_{th} , ideal particle pressure in the unsheared fluid, P_0 , and collision frequency, ω_c . They are given as a function of the experimental φ in (b), (c), and (d), respectively.

model, the dimensionless shear stress, $\sigma(\dot{\gamma}/\omega_0 | \varphi_{th})/P_0$, [Eq. (A8)] is parameterized by the packing fraction, φ_{th} , and uses properties of the unsheared fluid, namely, the collision frequency, ω_0 , and the ideal particle pressure, P_0 , as rate and stress scales, respectively. GITT predicts the rheological state diagram presented as inset of Fig. 4.

Given the qualitative similarity exhibited in Fig. 4, it is tempting to use the GITT relation as a constitutive model and fix its parameters by fitting. Note two things: firstly, we do not know the shear rate, $\dot{\gamma}(\Omega)$, in the shear thinning regime. To determine the non-linear mapping that applies there is beyond the scope of this letter [76], and we simply exclude the shear thinning regime from the fit. Secondly, although we measured the packing fraction, φ , we treat the packing fraction as a third fit parameter, φ_{th} . The glassy dynamics model, namely granular MCT [41], at the heart of GITT, is known to produce a finite offset, $\varphi - \varphi_{th} > 0$, to the experimental values of φ . This offset has hitherto not been quantified for granular fluidized beds.

In Fig. 5a we present the result of a manual fitting of the GITT constitutive model to our experimental flow curves. A detailed analysis of the fit parameters (Figs. 5b, c, d) is left for future work, but let us note that they all assume reasonable values and depend smoothly on the experimentally measured packing fraction, φ . The ability of the GITT constitutive model to capture both the Newtonian and Bagnold regimes, separated by many orders of magnitude in shear rate, shows that the ITT formalism extends to off-equilibrium dynamics, and further supports our scaling analysis of rheological regimes in air-fluidized granular beds, constituting the core of this contribution.

Conclusion.—We measure the rheology of a granular bed, agitated by air-fluidization, spanning five orders of magnitude in shear rate, $\dot{\gamma}$. We capture a diverse

rheology: Newtonian behavior at low $\dot{\gamma}$ and packing density, φ ; the development of an apparent dynamic yield stress around $\varphi_g = 0.6$, which we interpret as a granular glass transition; Bagnoldian shear thickening at high $\dot{\gamma}$, where σ collapses for all φ . The transitions between these regimes are characterized by two dimensionless numbers: the shear-to-fluidization power density ratio, Π , and the Péclet number, Pe . While $\Pi < 1$, the granular bed behaves akin to Brownian suspensions, $Pe = 1$ marking the shift from Newtonian to shear thinning behavior. At $\Pi > 1$, the material enters Bagnold regime, behaving like sheared, unfluidized granular media. These different regimes are qualitatively and quantitatively described by GITT, using underlying similarities between glasses, colloids, and granular matter to propose a unified approach to understanding the rheology of amorphous materials across scales.

With this work, we provide a framework to quantitatively characterize granular fluid's flow, on the same level as has been available for ordinary fluids. This will make granular flows amenable to continuum modeling in, e.g., industrial process design, geophysical hazard assessment, or predictions for environments challenging to access (e.g., for space exploration). More broadly, the approach presented here, relying on the importance of a glass transition and power balance, might apply more generally to non-equilibrium fluids, notably active and biological matter—a step towards a unified theoretical framework applicable from biological to astronomical systems.

Data availability statement.— The data that support the findings of this article are openly available [77]. The data shown in Fig. 1 was initially published in the doctoral thesis of O. D'Angelo (Ref. [78]).

Acknowledgements.— We are indebted to Dennis Schütz for sharing unpublished measurements that were the starting point of this study. We thank Miriam Siebenbürger and Abhishek Shetty for discussions on the experimental procedures, and Matthias Fuchs, Annette Zippelius and Olivier Coquand for companionship in the long development of GITT and many more interesting discussions. We thank Thomas Voigtmann for sharing rheological insight and steady encouragement.

-
- [1] D. Geldart, Types of gas fluidization, *Powder Technology* **7**, 285 (1973).
- [2] A. R. Abate and D. J. Durian, Approach to jamming in an air-fluidized granular bed, *Phys. Rev. E* **74**, 031308 (2006).
- [3] J. Werther, Fluidized-bed reactors, in *Ullmann's Encyclopedia of Industrial Chemistry* (John Wiley & Sons, Ltd, 2007).
- [4] Q. Guo, C. Spitler, J. M. Sanghishetty, and C. M. Boyce, Advances in vibrated gas-fluidized beds, *Current Opinion in Chemical Engineering* **42**, 100977 (2023).
- [5] C. Wilson, The role of fluidization in the emplacement of pyroclastic flows, 2: Experimental results and their interpretation, *Journal of Volcanology and Geothermal Research* **20**, 55 (1984).
- [6] H. J. Melosh, Dynamical weakening of faults by acoustic fluidization, *Nature* **379**, 601 (1996).
- [7] O. Roche, M. Gilbertson, J. Phillips, and R. Sparks, Experimental study of gas-fluidized granular flows with implications for pyroclastic flow emplacement, *Journal of Geophysical Research* **109**, 10.1029/2003JB002916 (2004).
- [8] E. C. P. Breard, J. Dufek, S. Charbonnier, V. Gueugneau, T. Giachetti, and B. Walsh, The fragmentation-induced fluidisation of pyroclastic density currents, *Nature Communications* **14**, 2079 (2023).
- [9] A. Kottlan, D. Schütz, and S. Radl, Rheological investigations on free-flowing and cohesive powders in different states of aeration, using a ball measuring system, *Powder Tech.* **338**, 783 (2018).
- [10] T. A. Brzinski III and D. J. Durian, Characterization of the drag force in an air-moderated granular bed, *Soft Matter* **6**, 3038 (2010).
- [11] É. Guazzelli and O. Pouliquen, Rheology of dense granular suspensions, *J. Fluid Mech.* **852** (2018).
- [12] P. Duru, M. Nicolas, J. Hinch, and É. Guazzelli, Constitutive laws in liquid-fluidized beds, *J. Fluid Mech.* **452**, 371 (2002).
- [13] L. G. Gibilaro, K. Gallucci, R. Di Felice, and P. Pagliai, On the apparent viscosity of a fluidized bed, *Chemical Engineering Science* **62**, 294 (2007).
- [14] C. Ancey and P. Coussot, Transition frictionnelle/visqueuse pour une suspension granulaire, *Comptes Rendus de l'Académie des Sciences - Series IIB - Mechanics-Physics-Astronomy* **327**, 515 (1999).
- [15] J. A. Dijkstra, G. H. Wortel, L. T. H. van Dellen, O. Dauchot, and M. van Hecke, Jamming, yielding, and rheology of weakly vibrated granular media, *Phys. Rev. Lett.* **107**, 108303 (2011).
- [16] C. Hanotin, S. Kiesgen de Richter, P. Marchal, L. J. Michot, and C. Baravian, Vibration-induced liquefaction of granular suspensions, *Phys. Rev. Lett.* **108**, 198301 (2012).
- [17] Z. Zhang, Y. Cui, D. H. Chan, and K. A. Taslagyan, DEM simulation of shear vibrational fluidization of granular material, *Granular Matter* **20**, 71 (2018).
- [18] A. Gnoli, A. Lasanta, A. Sarracino, and A. Puglisi, Unified rheology of vibro-fluidized dry granular media: From slow dense flows to fast gas-like regimes, *Scientific Reports* **6**, 38604 (2016).
- [19] N. J. van der Elst, E. E. Brodsky, P.-Y. Le Bas, and P. A. Johnson, Auto-acoustic compaction in steady shear flows: Experimental evidence for suppression of shear dilatancy by internal acoustic vibration, *J. Geophys. Res. Solid Earth* **117** (2012).
- [20] J. W. Conrad and J. Melosh, The rheology of acoustically fluidized sand, in *AGU Fall Meeting Abstracts*, Vol. 2013 (2013) pp. P41F–1986.
- [21] T. Hagyard and A. M. Sacerdote, Viscosity of suspensions of gas-fluidized spheres, *Ind. Eng. Chem. Fundamentals* **5**, 500 (1966).
- [22] E. Koos, E. Linares-Guerrero, M. L. Hunt, and C. E. Brennen, Rheological measurements of large particles in high shear rate flows, *Phys. Fluids* **24**, 013302 (2012).
- [23] V. Francia, L. A. A. Yahia, R. Ocone, and A. Ozel, From

- quasi-static to intermediate regimes in shear cell devices: Theory and characterisation, *KONA Powder Particle J.*, 2021018 (2021).
- [24] P. van den Leeden and G. J. Bouwhuis, Tentative rules for shearing stresses in particulate fluidized beds, *Appl. Sci. Res.* **10**, 78 (1961).
- [25] G. I. Tardos, M. I. Khan, and D. G. Schaeffer, Forces on a slowly rotating, rough cylinder in a couette device containing a dry, frictional powder, *Phys. Fluids* **10**, 335 (1998).
- [26] S. Chen, R. Cai, Y. Zhang, H. Yang, H. Zhang, and J. Lyu, A semi-empirical model to estimate the apparent viscosity of dense, bubbling gas-solid suspension, *Powder Technology* **377**, 289 (2021).
- [27] R. A. Bagnold, Experiments on a gravity-free dispersion of large solid spheres in a newtonian fluid under shear, *Proc. R. Soc. (London) A.* **225**, 49 (1954).
- [28] K. Schügerl, M. Merz, and F. Fetting, Rheologische Eigenschaften von Gasdurchströmten Fließbettssystemen, *Chem. Engng. Sci.* **15**, 1 (1961).
- [29] E. F. Hobbel and B. Scarlett, Measurement of the flow behaviour of aerated and fluidised powders using a rotating viscometer, *Particle & Particle Systems Characterization* **2**, 154 (1985).
- [30] J. Gottschalk, Rheological study of loosened bulk granular materials, *Particle & Particle Systems Characterization* **3**, 168 (1986).
- [31] A. B. Young, A. Shetty, and M. L. Hunt, Flow transitions and effective properties in an annular couette rheometer for gas fluidized beds and liquid-solid suspensions, submitted to *J. Fluid Mech.* (2021).
- [32] W. T. Kranz, F. Frahsa, A. Zippelius, M. Fuchs, and M. Sperl, Rheology of inelastic hard spheres at finite density and shear rate, *Phys. Rev. Lett.* **121**, 148002 (2018).
- [33] W. T. Kranz, F. Frahsa, A. Zippelius, M. Fuchs, and M. Sperl, Integration through transients for inelastic hard sphere fluids, *Phys. Rev. Fluids* **5**, 024305 (2020).
- [34] M. Fuchs and M. E. Cates, Theory of nonlinear rheology and yielding of dense colloidal suspensions, *Physical Review Letters* **89**, 248304 (2002).
- [35] L. M. C. Janssen, Mode-coupling theory of the glass transition: A primer, *Frontiers in Physics* **6**, 97 (2018).
- [36] $St := \rho_p du / \eta_f$, with the air's viscosity, η_f , and air flow velocity, u , are $\mathcal{O}(10^3)$.
- [37] J. M. Brader, T. Voigtmann, M. Fuchs, R. G. Larson, and M. E. Cates, Glass rheology: From mode-coupling theory to a dynamical yield criterion, *Proceedings of the National Academy of Sciences* **106**, 15186 (2009).
- [38] J. J. Stickel and R. L. Powell, Fluid mechanics and rheology of dense suspensions, *Annual Review of Fluid Mechanics* **37**, 129 (2005).
- [39] N. Wagner and J. Mewis, eds., *Theory and Applications of Colloidal Suspension Rheology*, Cambridge series in chemical engineering (Cambridge University Press, 2021).
- [40] M. I. Garcia de Soria, P. Maynar, and E. Trizac, Linear hydrodynamics for driven granular gases, *Phys. Rev. E* **87**, 022201 (2013).
- [41] W. T. Kranz, M. Sperl, and A. Zippelius, Glass transition for driven granular fluids., *Phys. Rev. Lett.* **104**, 225701 (2010).
- [42] I. M. Krieger and T. J. Dougherty, A mechanism for non-newtonian flow in suspensions of rigid spheres, *Trans. Soc. Rheol.* **3**, 137 (1959).
- [43] P. M. Reis, R. A. Ingale, and M. D. Shattuck, Caging dynamics in a granular fluid, *Phys. Rev. Lett.* **98**, 188301 (2007).
- [44] H. A. Barnes, The yield stress – a review or ‘panta roi’ – everything flows?, *J. Non-Newton. Fluid Mech.* **81**, 133 (1999).
- [45] G. Negro, L. N. Carenza, G. Gonnella, F. Mackay, A. Morozov, and D. Marenduzzo, Yield-stress transition in suspensions of deformable droplets, *Science Advances* **9**, eadf8106 (2023).
- [46] G. Katgert, A. Latka, M. E. Möbius, and M. van Hecke, Flow in linearly sheared two-dimensional foams: From bubble to bulk scale, *Phys. Rev. E* **79**, 066318 (2009).
- [47] K. N. Pham, G. Petekidis, D. Vlassopoulos, S. U. Egelhaaf, P. N. Pusey, and W. C. K. Poon, Yielding of colloidal glasses, *Europhysics Letters* **75**, 624 (2006).
- [48] A. Fall, F. m. c. Bertrand, G. Ovarlez, and D. Bonn, Yield stress and shear banding in granular suspensions, *Phys. Rev. Lett.* **103**, 178301 (2009).
- [49] P. Coussot, Structural similarity and transition from newtonian to non-newtonian behavior for clay-water suspensions, *Phys. Rev. Lett.* **74**, 3971 (1995).
- [50] R. Kostynick, H. Matinpour, S. Pradeep, S. Haber, A. Sauret, E. Meiburg, T. Dunne, P. Arratia, and D. Jerolmack, Rheology of debris flow materials is controlled by the distance from jamming, *Proceedings of the National Academy of Sciences* **119**, e2209109119 (2022).
- [51] S. Pradeep, P. E. Arratia, and D. J. Jerolmack, Origins of complexity in the rheology of soft earth suspensions, *Nature Comm.* **15**, 7432 (2024).
- [52] K. N. Pham, G. Petekidis, D. Vlassopoulos, S. U. Egelhaaf, W. C. K. Poon, and P. N. Pusey, Yielding behavior of repulsion- and attraction-dominated colloidal glasses, *Journal of Rheology* **52**, 649 (2008).
- [53] W. van Meegen, Crystallisation and the glass transition in suspensions of hard colloidal spheres, *Transp. Theory Stat. Phys.* **24**, 1017 (1995).
- [54] W. Götzke and T. Voigtmann, Effect of composition changes on the structural relaxation of a binary mixture, *Phys. Rev. E* **67**, 021502 (2003).
- [55] P. Coussot and C. Ancey, Rheophysical classification of concentrated suspensions and granular pastes, *Phys. Rev. E* **59**, 4445 (1999).
- [56] Precisely, we define the flow curve's inflection point, $\dot{\gamma}_0$, as $d^2 \ln \sigma / d(\ln \dot{\gamma})^2|_{\dot{\gamma}=\dot{\gamma}_0} = 0$.
- [57] We keep the notion of a Péclet number to stress the conceptual continuity between Brownian and non-Brownian agitated suspensions (see also e.g. [16, 55]); however, if we interpret τ as a structural rather than a diffusive time scale, one might be equally well justified to think of Pe as a Weissenberg number [34, 79].
- [58] S. L. Conway, T. Shinbrot, and B. J. Glasser, A Taylor vortex analogy in granular flows, *Nature* **431**, 433 (2004).
- [59] S. Khali, R. Nebbali, D. E. Ameziani, and K. Bouhadef, Numerical investigation of non-Newtonian fluids in annular ducts with finite aspect ratio using lattice Boltzmann method, *Phys. Rev. E* **87**, 053002 (2013).
- [60] P. Ramesh, S. Bharadwaj, and M. Alam, Suspension Taylor–couette flow: co-existence of stationary and traveling waves, and the characteristics of Taylor vortices and spirals, *J. Fluid Mech.* **870**, 901 (2019).
- [61] A. Dash, A. Anantharaman, and C. Poelma, Particle-laden Taylor–couette flows: higher-order transitions and evidence for azimuthally localized wavy vortices, *Journal*

- of Fluid Mechanics **903**, A20 (2020).
- [62] M. V. Majji, S. Banerjee, and J. F. Morris, Inertial flow transitions of a suspension in taylor–couette geometry, *J. Fluid Mech.* **835**, 936 (2018).
- [63] L. Baroudi, M. V. Majji, S. Peluso, and J. F. Morris, Taylor–couette flow of hard-sphere suspensions: overview of current understanding, *Philosophical Transactions of the Royal Society A: Mathematical, Physical and Engineering Sciences* **381**, 20220125 (2023).
- [64] We use the definition of DiPrima *et al.* [65], $Ta = \kappa Re^2$, where the prefactor $\kappa = 2(\delta - 1)/(\delta + 1)$ is related to the shear geometry.
- [65] R. C. DiPrima, P. M. Eagles, and B. S. Ng, The effect of radius ratio on the stability of couette flow and taylor vortex flow, *Phys. Fluids* **27**, 2403 (1984).
- [66] J. J. J. Gillissen and H. J. Wilson, Effect of normal contact forces on the stress in shear rate invariant particle suspensions, *Phys. Rev. Fluids* **4**, 013301 (2019).
- [67] E. Brown and H. M. Jaeger, Shear thickening in concentrated suspensions: phenomenology, mechanisms and relations to jamming, *Reports on progress in physics* **77**, 10.1088/0034-4885/77/4/046602 (2014).
- [68] A. Lemaître, J.-N. Roux, and F. Chevoir, What do dry granular flows tell us about dense non-brownian suspension rheology?, *Rheol. Acta* **48**, 925 (2009).
- [69] N. Y. C. Lin, B. M. Guy, M. Hermes, C. Ness, J. Sun, W. C. K. Poon, and I. Cohen, Hydrodynamic and contact contributions to continuous shear thickening in colloidal suspensions, *Phys. Rev. Lett.* **115**, 228304 (2015).
- [70] J. F. Morris, Lubricated-to-frictional shear thickening scenario in dense suspensions, *Phys. Rev. Fluids* **3**, 110508 (2018).
- [71] S. Jamali and J. F. Brady, Alternative frictional model for discontinuous shear thickening of dense suspensions: Hydrodynamics, *Phys. Rev. Lett.* **123**, 138002 (2019).
- [72] A. Lemaître, Origin of a repose angle: Kinetics of rearrangement for granular materials, *Phys. Rev. Lett.* **89**, 064303 (2002).
- [73] Y. Forterre and O. Pouliquen, Flows of dense granular media, *Annual Review of Fluid Mechanics* **40**, 10.1146/annurev.fluid.40.111406.102142 (2008).
- [74] Y. Madraki, A. Oakley, A. Nguyen Le, A. Colin, G. Ovarlez, and S. Hormozi, Shear thickening in dense non-brownian suspensions: Viscous to inertial transition, *J. Rheol.* **64**, 227 (2020).
- [75] F. Tapia, M. Ichihara, O. Pouliquen, and E. Guazzelli, Viscous to inertial transition in dense granular suspension, *Phys. Rev. Lett.* **129**, 078001 (2022).
- [76] O. D’Angelo, A. Shetty, M. Sperl, and W. T. Kranz, The manifold rheology of fluidized granular media (2024), unpublished.
- [77] O. D’Angelo, M. Sperl, and W. T. Kranz, [Dataset] Rheological regimes in agitated granular media under shear, Zenodo dataset 13628373 (2024).
- [78] O. Lopez D’Angelo, *Powder-based additive manufacturing for space*, Phd dissertation, Aachen, Germany (2021).
- [79] J. L. White, Dynamics of viscoelastic fluids, melt fracture, and the rheology of fiber spinning, *J. Appl. Polymer Sci.* **8**, 2339 (1964).
- [80] C. Kang and P. Mirbod, Flow instability and transitions in taylor–couette flow of a semidilute non-colloidal suspension, *Journal of Fluid Mechanics* **916**, A12 (2021).
- [81] S. Wroński and M. Jastrzebski, Experimental investigations of the stability limit of the helical flow of pseudo-plastic liquids, *Rheol. Acta* **29**, 453 (1990).
- [82] M. Jastrzebski, H. Zaidani, and S. Wroński, Stability of couette flow of liquids with power law viscosity, *Rheol. Acta* **31**, 264 (1992).
- [83] J. P. Pascal and H. Rasmussen, Stability of power law fluid flow between rotating cylinders, *Dyn. Stability Sys.* **10**, 65 (1995).

Appendix I: Methods

Rheometry.—The rheometry setup is an open-surface Taylor-Couette (coaxial cylinders, inner cylinder rotating). The surface of the inner cylinder promotes particle-particle contact during shear (Fig. A1a).

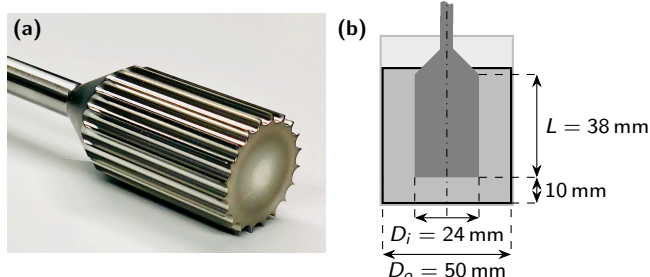


FIG. A1. Rheometry setup. (a) Profiled inner cylinder. (b) Shear cell dimensions (section view), with inner and outer cylinders diameter, $D_{i,o}$, respectively.

Packing fractions.—The global packing fraction is determined as $\varphi(u) = M/\rho_p V(u)$, where the sample volume is obtained from the fluidization-dependent mean bed height, $h(u)$, determined by image analysis.

The fit function to $\varphi(u)$, shown as inset of Fig. 1, is of form $\varphi = (Au)^{-B}$, with $A = 91\,960\text{ s m}^{-1}$, $B = 0.068$.

Appendix II: Strain constants

In the stationary state, forces in a fluid must balance, i.e., in terms of the stress tensor, $\underline{\sigma}$, we have $\nabla \cdot \underline{\sigma} = 0$. Focusing on the shear stress $\sigma(r) := \sigma_{r,\vartheta}(r)$, neglecting other shear components and assuming a homogeneous pressure, this reads

$$(\nabla \cdot \underline{\sigma})_{\vartheta} := \frac{\partial \sigma(r)}{\partial r} + \frac{2\sigma(r)}{r} = 0. \quad (\text{A1})$$

In terms of the measured stress at the inner cylinder, $\sigma \equiv \sigma(R_i)$, this implies $\sigma(r) = (R_i/r)^2 \sigma$, i.e., the shear stress decreases quadratically towards the outer cylinder.

Assuming no-slip boundary conditions, the angular velocity $\Omega(r)$ is fixed at the cylinders surfaces, $\Omega(R_i) = \Omega$ and $\Omega(R_o) = 0$. The shear rate is related to the gradient of the angular velocity, $\dot{\gamma}(r) = r d\Omega(r)/dr$, such that

$$\Omega = \int_{R_i}^{R_o} dr \frac{d\Omega}{dr} = \int_{R_i}^{R_o} dr \frac{\dot{\gamma}(r)}{r} = \int_{\sigma/\delta^2}^{\sigma} \frac{\dot{\gamma}(s) ds}{2s}. \quad (\text{A2})$$

Using Newtonian rheology, $\dot{\gamma}(\sigma) = \sigma/\eta$, we find

$$\eta = \frac{\delta^2 - 1}{2\delta^2} \times \frac{\sigma}{\Omega} \quad (\text{A3})$$

and recover the well-known strain constant for the Taylor-Couette geometry,

$$\dot{\gamma}_N = \frac{2\delta^2}{\delta^2 - 1} \Omega. \quad (\text{A4})$$

Assuming Bagnold rheology, instead, $\dot{\gamma}(\sigma) = \sqrt{\sigma/B}$, Eq. (A2) yields

$$B = \frac{(\delta - 1)^2}{\delta^2} \times \frac{\sigma}{\Omega^2} \quad (\text{A5})$$

and, respectively, the strain constant

$$\dot{\gamma}_B = \frac{\delta}{\delta - 1} \Omega. \quad (\text{A6})$$

Appendix III: Taylor instability

For dense granular suspensions sheared in a Taylor-Couette geometry, the critical Reynolds number above which flow instabilities appear $\text{Re}_c \sim \mathcal{O}(100)$ [55, 60–63, 80]. Throughout our experiment, we strictly find $\text{Re} < 10$ (see Fig. A2), suggesting circular Couette flow (laminar).

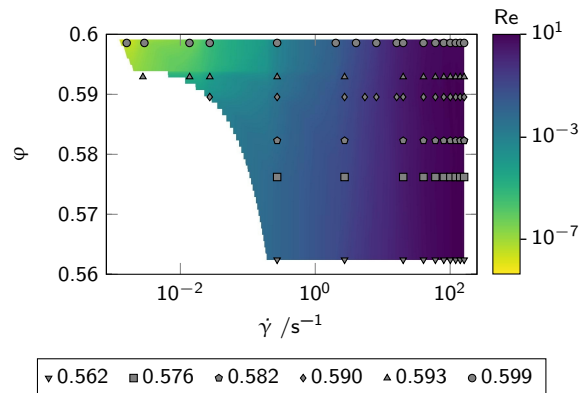


FIG. A2. Reynolds number, Re , calculated on the experiment parameter space, versus shear rate, $\dot{\gamma}$, and packing fraction, φ . Marks are the measured datapoints.

The dimensionless Taylor number, Ta , that compares the Coriolis to viscous forces, depends, besides the shear geometry, on the rotation rate, Ω , and the kinetic viscosity, $\nu := \eta/\rho_b \varphi$. We use the definition proposed by DiPrima *et al.* [65]:

$$\text{Ta} = 2 \frac{(\delta - 1)}{(\delta + 1)} \left(\frac{\Omega R_i (R_o - R_i)}{\nu} \right)^2 = \kappa \text{Re}^2. \quad (\text{A7})$$

Other definitions have been used [61, 66, 81–83]; for $\text{Ta} = \kappa \text{Re}^2$, generally $\kappa \sim \mathcal{O}(1)$.

The critical Taylor number Ta_c depends on the nature of the fluid and shear geometry. The influence of the geometry is rather well understood in case of Newtonian

fluids, with wider gaps having a higher Ta_c [65]. For non-Newtonian fluids, $\eta \propto \dot{\gamma}^{R \neq 0}$, the dependence of Ta_c on the flow index, R , is mostly investigated for shear thinning or at most mildly shear thickening fluids [81–83]. We are not aware of explicit results for $R = 1$, relevant for our Bagnold regime, and particle concentration has yielded contradictory results [61, 63, 66].

For non-Brownian suspensions at relatively high particle concentration ($\varphi = 0.5$), Dash *et al.* [61] define $\text{Ta} \propto \text{Re}^2$ and measure $\text{Ta}_c \sim \mathcal{O}(10^5)$. Others [62, 65, 66] define $\text{Ta} \propto \text{Re}$ and find that the onset of Taylor instability happens at $\text{Ta}_c \sim \mathcal{O}(50)$, translating in our definition to $\text{Ta}_c \sim \mathcal{O}(10^3)$. For lack of (i) a widely accepted definition of Ta , (ii) a clear critical value Ta_c , and (iii) understanding of the evolution of Ta_c for non-Newtonian suspensions, we consider that following our definition, $\text{Ta} < 10^3 \lesssim \text{Ta}_c$ seem to indicate that the shear thickening regime observed cannot be explained by the Taylor instability.

Appendix IV: Constitutive relation

The granular integration through transient (GITT) [32, 33] formalism takes into account the scaling analysis presented in the main text, to provide a dimensionless constitutive relation for dissipative smooth hard sphere in

terms of a generalized Green-Kubo integral,

$$\begin{aligned} & \sigma(\dot{\gamma}/\omega_0 | \varphi)/P_0 \\ &= \frac{\dot{\gamma}}{\omega_0} \frac{T}{T_0} \sum_{\mathbf{q}} \int_0^\infty d(\omega_0 t) \mathcal{V}_{\mathbf{q}\mathbf{q}(-t)} \Phi_{\mathbf{q}(-t)}^2(t), \quad (\text{A8}) \end{aligned}$$

where P_0 , ω_0 are the ideal particle pressure and collision frequency in the unsheared fluidized bed, respectively.

The stress-density coupling constant, $V_{\mathbf{q}\mathbf{q}(-t)}$, is known explicitly [33]. In addition to the explicit shear rate dependence of the above relation, the shear rate also affects the advection of the wave vectors, $\mathbf{q}(-t)$, and the density correlator, $\Phi_{\mathbf{q}}(t)$, allowing for non-Newtonian rheology [33, 34].

The constitutive equation (Eq. A8) uses the packing fraction, φ , to uniquely characterize the granular fluid. Note however that the shape of the GITT constitutive relation depends weakly on one more parameter [32], the coefficient of restitution, ε , which we fix here to $\varepsilon = 0.8$. The granular temperature, T , in the sheared stationary state is determined by the power density balance,

$$\Pi_{\dot{\gamma}}(T) + \Pi_f = \Pi_c(T). \quad (\text{A9})$$